Estimation of fracture indicators using azimuthal PP-wave amplitudes without NMO correction

Huaizhen Chen[*] and Kristopher A. Innanen

ABSTRACT

Seismic waveforms at large offsets are stretched during NMO correction, which are usually muted in seismic processing. However, in horizontal vertically isotropic (HTI) media or hydrocarbon reservoirs with vertical fractures, variation of seismic wave reflection with azimuthal angle is more obvious at large offsets, which means seismic waveforms of large offsets are indispensable to implement a better characterization of HTI media and fractured reservoirs. To circumvent the NMO stretching and reserve seismic waveforms at large offsets, we present an approach and workflow of employing seismic waveforms without NMO correction to estimate elastic impedance EI and fracture parameters (i.e. fracture weaknesses). Starting with re-expression of P- and S-wave velocities of HTI media, we derive PP-wave reflection coefficient and azimuthal EI as a function of the normal and tangential fracture weaknesses based on the solution of Zoeppritz equations. Using the derived azimuthal EI, we introduce a NMO operator to the convolution model to generate PP-wave seismic data without NMO correction. A two-step inversion workflow is established to estimate fracture weaknesses using seismic data, which is implemented as: 1) using seismic data without NMO correction at different incidence and azimuthal angles to invert for EI, and 2) using difference in EI at different azimuthal angles as input data to estimate fracture weaknesses. Bayesian inversion algorithm is employed in the two-step inversion. Synthetic seismic data of signal-to-noise ratio (SNR) of 2 is generated to verify the robustness of the proposed inversion approach. In the case of applying the proposed inversion approach and workflow to real datasets acquired over fractured reservoirs, reliable results of fracture weaknesses are obtained, which may guide the identification of potential fractured reservoirs.

INTRODUCTION

P-wave velocity changes with the angle of incidence and azimuth in horizontal transversely isotropic (HTI) media. Tsvankin (1997) presents P-wave velocity as a function of weak-anisotropy parameters (ϵ, δ), and Rüger (1996, 1998) derives the incidence and azimuthal angle dependent P-wave velocity that is also expressed in terms of weak-anisotropy parameters in HTI media. By analyzing P-wave velocity variation with the angle of incidence and azimuth (VVAZ), weak-anisotropy parameters are estimated (Jenner, 2010).

To understand how cracks affect rock elastic properties, Hudson (1980) presents a penny-shaped cracked model and proposes two displacement parameters U_{11} and U_{33} that are related to crack density and bulk modulus of infilled fluids. For rocks containing relatively large scale fractures, Schoenberg and Protazio (1992); Schoenberg and Sayers (1995) present a linear-slip model that involves fracture compliances (Z_N and Z_T) or weaknesses

---
[*]School of Ocean and Earth Science, Tongji University, Shanghai, China; and CREWES Project, University of Calgary, Calgary, Alberta, Canada. Email: huaizhen.chen@ucalgary.ca

(δ_N and δ_T) to stiffness matrix of rocks. Combining the penny-shaped model and the linear-slip model, Bakulin et al. (2000) present fracture weaknesses as a function of displacement parameters, which relates fracture weaknesses to fracture density and bulk and shear moduli of fracture fillings. Using the linear-slip model, weak-anisotropy parameters are expressed in terms of fracture weaknesses, and the incidence- and azimuthal-angle-dependent P-wave velocity can also be re-expressed as a function of fracture weaknesses. This makes it possible to use P-wave VVAZ to predict fracture weaknesses directly.

Starting with re-parameterization of P-wave velocity in HTI media, Rüger (1996) derives P-to-P and P-to-S wave reflection coefficients and analyzes how seismic wave reflection amplitude varies with the angle of incidence and azimuth (AVAZ). The derived reflection coefficients promote the prediction of underground hydrocarbon-bearing fractured reservoirs using seismic datasets of different incidence and azimuthal angles. Using the P-to-P wave reflection coefficient given by Rüger (1996), Downton and Benjamin (2010) implement the simultaneous inversion for elastic parameters (P- and S-wave impedances) and fracture weaknesses (δ_N and δ_T) using azimuthal seismic datasets. Based on the model of fluid substitution in anisotropic media and the linear-slip model, Chen and Zhang (2017) and Chen et al. (2018) present a new 'solid-fluid-fracture' decoupled PP-wave reflection coefficient as a function of elastic properties of isotropic background rock, fluid indicators and dry fracture weaknesses, and based on the 'solid-fluid-fracture' decoupled reflection coefficient, the estimation of dry fracture weaknesses and fluid indicators using azimuthal seismic data is implemented. However, in HTI media, variation of seismic wave reflection with azimuthal angle is more obvious at large incidence angles. To implement a better estimation of underground hydrocarbon-bearing fractured reservoirs, seismic waveforms of large offsets are required. However, seismic waveforms of large offsets are usually muted due to NMO stretching. In the present study, we aim to establish an inversion approach and workflow of employing azimuthal seismic datasets without NMO correction to estimate fracture weaknesses, which may combine features of AVAZ and VVAZ to improve the accuracy of inversion for fracture weaknesses.

Using the incidence- and azimuthal-angle-dependent P- and S-wave velocities given by Rüger (1996) and Tsvankin and Thomsen (1995), we first re-express P- and S-wave velocities in HTI media as a function of fracture weaknesses δ_N and δ_T. Based on the solution of Zoeppritz equations, we present PP-wave reflection coefficient and azimuthal elastic impedance (EI) in terms of δ_N and δ_T, and accuracy of the PP-wave reflection coefficient is verified using a two-layered fractured model in the case of different incidence and azimuthal angles. Using the derived azimuthal EI, we introduce a NMO operator to re-express the convolution model to generate seismic gathers without NMO correction. A two-step inversion workflow is proposed, which involves the inversion for azimuthal EI using seismic gathers without NMO correction and the estimation of fracture weaknesses using azimuthal differences in the inverted EI datasets. Synthetic seismic gathers of signal-to-noise ratio (SNR) of 2 are used to verify the robustness of the proposed inversion approach. We finally apply the proposed inversion approach and workflow to real data acquired over fractured reservoirs, and reliable results of fracture weaknesses are obtained, which provides valuable information for the detection of potential fractured reservoirs.

THEORY AND METHOD

In this section, we first present incidence- and azimuthal-angle-dependent P- and S-wave velocities in terms of fracture weaknesses in HTI media, and then we derive P-to-P wave reflection coefficient in terms of fracture weaknesses based on the solution of Zoeppritz equations. We propose an inversion approach and workflow of employing azimuthal PP-wave amplitudes without NMO correction to estimate fracture weaknesses.

Re-derivation of PP-wave reflection coefficient in HTI media

In the case that rocks contain a set of vertically aligned fractures whose normals are parallel to x_1-axis, Rüger (1996) and Tsvankin and Thomsen (1995) present incidence- and azimuthal-angle-dependent P- and S-wave velocities of HTI media in terms of anisotropic parameters (ε, δ and γ)

$$V_{\mathrm{P}}\left(\theta, \phi\right) = \alpha \left(1 + \delta \sin^2 \theta \cos^2 \theta \cos^2 \phi + \varepsilon \sin^4 \theta \cos^4 \phi\right),$$

$$V_{\mathrm{S}}\left(\theta, \phi\right) = \beta \left(1 - \frac{1}{g}\delta \sin^2 \theta \cos^2 \theta \cos^2 \phi + \frac{1}{g}\varepsilon \sin^2 \theta \cos^2 \theta \cos^4 \phi\right),$$

(1)

where α and β are P- and S-wave velocities of the isotropic background rock, θ is incidence angle, and ϕ is azimuthal angle.

Bakulin et al. (2000) present approximate relationships between anisotropic parameters and fracture weaknesses (δ_{N} and δ_{T}) as

$$\varepsilon = -2g\left(1 - g\right)\delta_{\mathrm{N}}$$

$$\delta = -2g\left[\left(1 - 2g\right)\delta_{\mathrm{N}} + \delta_{\mathrm{T}}\right]$$

(2)

$$\gamma = -\frac{\delta_{\mathrm{T}}}{2},$$

where δ_{N} and δ_{T} are the normal and tangential fracture weaknesses, which are related to fracture properties (e.g. fracture density and fluid bulk modulus).

Combining equations 1 and 2, we rewrite the P- and S-wave velocities in terms of fracture weaknesses as

$$
\begin{aligned}
V_{\mathrm{P}}\left(\theta, \phi\right) \approx & \, \alpha \left\{1 - 2g\left[\left(1 - 2g\right)\cos^2 \theta + \left(1 - g\right)\sin^2 \theta \cos^2 \phi\right]\sin^2 \theta \cos^2 \phi \, \delta_{\mathrm{N}}\right. \\
& \left. -2g \sin^2 \theta \cos^2 \theta \cos^2 \phi \, \delta_{\mathrm{T}}\right\},
\end{aligned}
$$

(3)

$$
\begin{aligned}
V_{\mathrm{S}}\left(\theta, \phi\right) \approx & \, \beta \left\{1 + 2\left[\left(1 - 2g\right) - \left(1 - g\right)\cos^2 \phi\right]\sin^2 \theta \cos^2 \theta \cos^4 \phi \, \delta_{\mathrm{N}}\right. \\
& \left. +2\sin^2 \theta \cos^2 \theta \cos^2 \phi \, \delta_{\mathrm{T}}\right\}.
\end{aligned}
$$

For an interface separating two HTI media, we express the S-wave velocity of the back-

ground rock and the fracture indicator across the interface as

$$\alpha_1 = \overline{\alpha}(1 - r_\alpha), \ \alpha_2 = \overline{\alpha}(1 + r_\alpha),$$

$$\beta_1 = \overline{\beta}(1 - r_\beta), \ \beta_2 = \overline{\beta}(1 + r_\beta),$$

$$\rho_1 = \overline{\rho}(1 - r_\rho), \ \rho_2 = \overline{\rho}(1 + r_\rho),$$

$$\delta_{N1} = \overline{\delta}_N(1 - r_{\delta_N}), \ \delta_{N2} = \overline{\delta}_N(1 + r_{\delta_N}),$$

$$\delta_{T1} = \overline{\delta}_T(1 - r_{\delta_T}), \ \delta_{T2} = \overline{\delta}_T(1 + r_{\delta_T}), \tag{4}$$

where $r_\alpha = \frac{\Delta\alpha}{2\overline{\alpha}}$, $r_\beta = \frac{\Delta\beta}{2\overline{\beta}}$, $r_\rho = \frac{\Delta\rho}{2\overline{\rho}}$, $r_{\delta_N} = \frac{\Delta\delta_N}{2\overline{\delta}_N}$, $r_{\delta_T} = \frac{\Delta\delta_T}{2\overline{\delta}_T}$, $\overline{\alpha}$, $\overline{\beta}$, $\overline{\rho}$, $\overline{\delta}_N$ and $\overline{\delta}_T$ are P- and S-wave velocities, density and fracture weaknesses in the background media, and $\Delta\alpha$, $\Delta\beta$, $\Delta\rho$, $\Delta\delta_N$ and $\Delta\delta_T$ are changes in P- and S-wave velocities, density and fracture weaknesses across the reflection interface. Substituting equation 4 to equation 3, we may derive P- and SV-wave velocities of the upper and lower fractured layers, which can be expressed as functions of reflectivities r_α, r_β, r_ρ, r_{δ_N} and r_{δ_T}.

Zoeppritz equations are solved to obtain reflection and transmission coefficients of plane waves (Aki and Richards, 2002). Ikelle and Amundsen (2018) present explicit expressions of reflection coefficients using P- and S-wave velocities for a reflection interface separating two isotropic media. PP-wave reflection coefficient R_{PP} is given by (Ikelle and Amundsen, 2018)

$$R_{PP} = \frac{c_1 d_2 - c_3 d_4}{d_1 d_2 + d_4 d_3}, \tag{5}$$

where

$$d_1 = 2K^2 \Delta G \left(\sqrt{V_{P1}^{-2} - K^2} - \sqrt{V_{P2}^{-2} - K^2} \right) + \left(\rho_1 \sqrt{V_{P2}^{-2} - K^2} + \rho_2 \sqrt{V_{P1}^{-2} - K^2} \right),$$

$$d_2 = 2K^2 \Delta G \left(\sqrt{V_{S1}^{-2} - K^2} - \sqrt{V_{S2}^{-2} - K^2} \right) + \left(\rho_1 \sqrt{V_{S2}^{-2} - K^2} + \rho_2 \sqrt{V_{S1}^{-2} - K^2} \right),$$

$$d_3 = K \left[2\Delta G \left(\sqrt{V_{P1}^{-2} - K^2}\sqrt{V_{S2}^{-2} - K^2} + K^2 \right) + \Delta\rho \right],$$

$$d_4 = K \left[2\Delta G \left(\sqrt{V_{P2}^{-2} - K^2}\sqrt{V_{S1}^{-2} - K^2} + K^2 \right) + \Delta\rho \right],$$

$$c_1 = 2K^2 \Delta G \left(\sqrt{V_{P1}^{-2} - K^2} + \sqrt{V_{P2}^{-2} - K^2} \right) - \left(\rho_1 \sqrt{V_{P2}^{-2} - K^2} - \rho_2 \sqrt{V_{P1}^{-2} - K^2} \right),$$

$$c_3 = -K \left[2\Delta G \left(\sqrt{V_{P1}^{-2} - K^2}\sqrt{V_{S2}^{-2} - K^2} - K^2 \right) - \Delta\rho \right], \tag{6}$$

Table 1. P- and S-wave velocities, density and fracture weaknesses of two fractured layers

	α (m/s)	β (m/s)	ρ (g/cm^3)	δ_{N}	δ_{T}	ε	δ	γ
Layer 1	5000	2800	2.25	0.02	0.01	-0.009	-0.011	-0.005
Layer 2	4000	2300	2.3	0.6	0.35	-0.266	-0.366	-0.175

where $\Delta G = \rho_1 (V_{\mathrm{S}1})^2 - \rho_2 (V_{\mathrm{S}2})^2$ is the difference between shear moduli of upper and lower fractured layers, $V_{\mathrm{P}1}$ and $V_{\mathrm{P}2}$ are P-wave velocities of the upper and lower fractured layers, $K = \frac{\sin \theta_{\mathrm{P}1}}{V_{\mathrm{P}1}} = \frac{\sin \theta_{\mathrm{P}2}}{V_{\mathrm{P}2}}$ is the approximate ray parameter in anisotropic media, in which $\theta_{\mathrm{P}1}$ and $\theta_{\mathrm{P}2}$ are angles of reflected and transmitted P waves in the upper and lower layers, respectively.

Chen et al. (2018) present the approximate form of Snell's law is applicable in anisotropic media for the case of small fracture weaknesses. In the present study, we derive PP-wave reflection coefficient (R_{PP}) also for the case of small normal and tangential fracture weaknesses (i.e. $\delta_{\mathrm{N}} \ll 1$ and $\delta_{\mathrm{T}} \ll 1$) and under the assumption of small changes in elastic properties and fracture weaknesses across the reflection interface. It indicates that we may neglect the term proportional to $\Delta G \Delta \rho$, $(\Delta G)^2$, and $(\Delta \rho)^2$ in the derivation of R_{PP}. Therefore, R_{PP} in equation 5 is simplified as

$$
\begin{aligned}
R_{\mathrm{PP}} (\theta, \phi) &\approx \frac{c_1}{d_1} \\
&\approx a_{\mathrm{p}} (\theta) \, r_{\mathrm{p}} + a_{\mathrm{s}} (\theta) r_{\mathrm{s}} + a_{\mathrm{d}} (\theta) r_{\mathrm{d}} \\
&\quad + a_{\mathrm{N}} (\theta, \phi) \Delta \delta_{\mathrm{N}} + a_{\mathrm{T}} (\theta, \phi) \Delta \delta_{\mathrm{T}},
\end{aligned} \tag{7}
$$

where

$$
a_{\mathrm{p}} (\theta) = \sec^2 \theta,
$$

$$
a_{\mathrm{s}} (\theta) = -8g \sin^2 \theta,
$$

$$
a_{\mathrm{d}} (\theta) = 1 - 4g \sin^2 \theta,
$$

$$
a_{\mathrm{N}} (\theta, \phi) = -g \sin^2 \theta \cos^2 \theta \cos^2 \phi \left[\begin{matrix} (1 - 2g) \left(8 \sin^2 \theta \cos^2 \phi + 1 \right) \\ + (1 - g) \tan^2 \theta \left(1 - 8 \cos^2 \theta \cos^2 \phi \right) \cos^2 \phi \end{matrix} \right],
$$

$$
a_{\mathrm{T}} (\theta, \phi) = -g \sin^2 \theta \cos^2 \theta \cos^2 \phi \left(8 \sin^2 \theta + 1 \right), \tag{8}
$$

and where θ is the average of P-wave incidence and transmission angles.

We next use a model of an interface separating two-layer fractured model to calculate PP-wave reflection coefficient using our new derived R_{PP} (equation 7), R_{PP} obtained from the solution of Zoeppritz equations (equation 5) and the reflection coefficient proposed by Rüger (1996). In Table 1, we show elastic parameters (P- and S-wave velocities of the isotropic background), fracture weaknesses, and weak anisotropic parameters that are computed using fracture weaknesses as shown in equation 2.

Comparisons between results of R_{PP} calculated using different equations in the case of different incidence and azimuthal angles are shown in Figure 1. We observe that R_{PP}
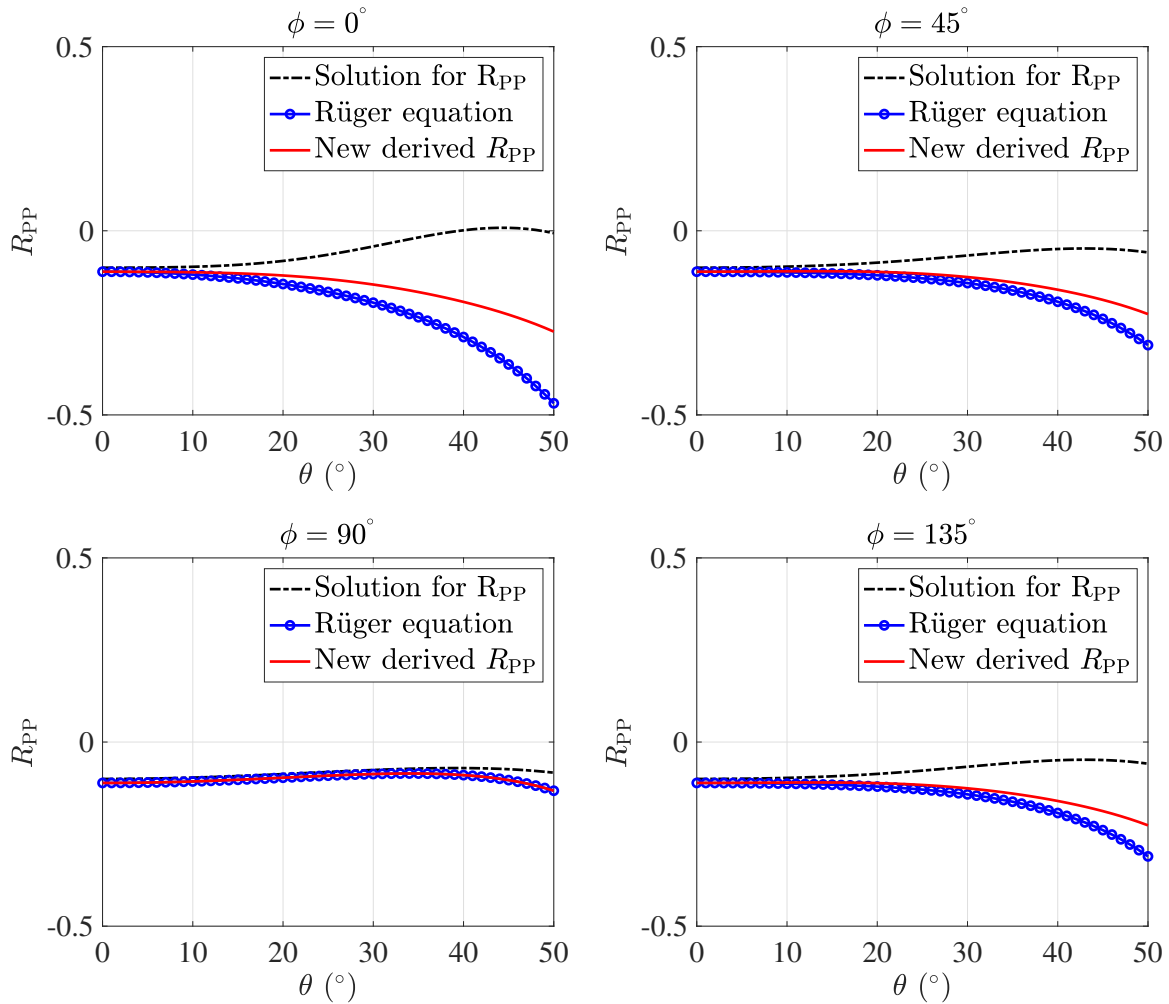
FIG. 1. Comparisons between results of R_{PP} calculated using different equations in the case of different incidence and azimuthal angles. Dashed curve represents R_{PP} calculated using the solution of Zoeppritz equations, red curve represents R_{PP} calculated using the new derived reflection coefficient, and blue circle represents R_{PP} computed using Rüger's equation.

generated using the new derived reflection coefficient is closer to results of R_{PP} computed using solution of Zoeppritz equations than that calculated using Rüger's equation. It verifies the accuracy of the new derived reflection coefficient and illustrate the new derived R_{PP} can be used in the next inversion of seismic data for estimating fracture weaknesses.

Generation of synthetic seismic gathers without NMO correction

Chen et al. (2018) present an azimuthal elastic impedance (EI) as a function of fracture weaknesses. Using the approximate relation that $R_{\mathrm{PP}} \approx \Delta \mathrm{EI}/(2\,\mathrm{EI})$, we present a new expression of azimuthal EI based on the derived reflection coefficient

$$\mathrm{EI}\,(\theta, \phi) = \alpha^{a_{\mathrm{P}}(\theta)}\,\beta^{a_{\mathrm{s}}(\theta)}\,\rho^{a_{\mathrm{d}}(\theta)}\,\exp\left[2a_{\mathrm{N}}\,(\theta, \phi)\delta_{\mathrm{N}} + 2a_{\mathrm{T}}\,(\theta, \phi)\delta_{\mathrm{T}}\right], \qquad (9)$$

and based on the derived reflection coefficient and azimuthal EI, we next re-express the convolution model and show how to generate PP-wave seismic data without NMO correction.

Following Claerbout (2004), we present an azimuthal AVA NMO model to generate synthetic pre-stacked seismic data, in which we involve a NMO operator to produce synthetic gather without NMO correction. In the case of n reflection interfaces and l incidence angles, the synthetic seismic gather without NMO correction is generated using P-wave wavelet and PP-wave azimuthal EI

$$\mathbf{s} = \mathbf{A}\,\mathbf{e} = \mathbf{W}\,\mathbf{N}\,\mathbf{D}\,\mathbf{e}, \tag{10}$$

where $\mathbf{N}$ is a NMO operator that is related to incidence- and azimuthal-angle-dependent velocity $V_{\mathrm{P}}(\theta, \phi)$, $\mathbf{D}$ is difference matrix, and $\mathbf{s}$, $\mathbf{W}$ and e are vectors of seismic gather, wavelet and azimuthal EI, which are given by

$$\mathbf{s} = \begin{bmatrix} \mathbf{s}_1 & & & & & \\ & \mathbf{s}_2 & & & & \\ & & \ddots & & & \\ & & & \mathbf{s}_i & & \\ & & & & \ddots & \\ & & & & & \mathbf{s}_n \end{bmatrix}_{n \times ln},$$

$$\mathbf{W} = \begin{bmatrix} w_1 & & & & \\ w_2 & w_1 & & & \\ \vdots & w_2 & \ddots & & \\ \vdots & \vdots & \ddots & \ddots & \\ w_n & \cdots & \cdots & w_2 & w_1 \end{bmatrix}_{n \times n},$$

$$\mathbf{D} = \begin{bmatrix} -\frac{1}{2} & \frac{1}{2} & & & & \\ & & -\frac{1}{2} & \frac{1}{2} & & \\ & & & \ddots & \ddots & \\ & & & & -\frac{1}{2} & \frac{1}{2} \end{bmatrix}_{ln \times 2ln},$$

$$\mathbf{e} = \begin{bmatrix} \mathbf{e}_1 & & & & & \\ & \mathbf{e}_2 & & & & \\ & & \ddots & & & \\ & & & \mathbf{e}_i & & \\ & & & & \ddots & \\ & & & & & \mathbf{e}_n \end{bmatrix}_{2ln \times ln}, \tag{11}$$

where

$$\mathbf{s}_i = \begin{bmatrix} s(t_i, \theta_1, \phi) & s(t_i, \theta_2, \phi) & \cdots & s(t_i, \theta_l, \phi) \end{bmatrix}_{1 \times l},$$

$$
\mathbf{e}_i =
\begin{bmatrix}
\ln \mathrm{EI}\left(t_i, \theta_1, \phi\right) & & & & & \\
\ln \mathrm{EI}\left(t_{i+1}, \theta_1, \phi\right) & & & & & \\
& \ln \mathrm{EI}\left(t_i, \theta_2, \phi\right) & & & & \\
& \ln \mathrm{EI}\left(t_{i+1}, \theta_2, \phi\right) & & & & \\
& & \ddots & & & \\
& & & \ddots & & \\
& & & & \ln \mathrm{EI}\left(t_i, \theta_l, \phi\right) & \\
& & & & \ln \mathrm{EI}\left(t_{i+1}, \theta_l, \phi\right) &
\end{bmatrix}_{2l \times l}, \qquad (12)
$$

in which $s\left(t_i, \theta_1, \phi\right), ..., s\left(t_i, \theta_l, \phi\right)$ and $\ln \mathrm{EI}\left(t_i, \theta_1, \phi\right), ..., \ln \mathrm{EI}\left(t_i, \theta_l, \phi\right)$ represent time samples of seismic data and logarithmic azimuthal EI of incidence angles $\theta_1, ..., \theta_l$ and azimuth ϕ, respectively. The NMO operator $\mathbf{N}$ is computed using the expressed P-wave velocity shown in equation 3.

Inversion of azimuthal PP-wave amplitudes without NMO correction for estimating fracture weaknesses

Based on different parameterized EI, the two-step inversion approach is established for estimating elastic parameters and anisotropic parameters (Martins, 2006; Zong et al., 2013; Chen et al., 2018). It is implemented as: 1) employing seismic angle gathers to estimate EI datasets of different incidence angles; and 2) using the estimated EI datasets to predict elastic and anisotropic parameters.

In the present study, we first input azimuthal PP-wave seismic data to estimate azimuthal EI datasets, and then we implement the inversion of azimuthal EI datasets for predicting fracture weaknesses. The novelty of our inversion approach is we employ the difference between EI of different azimuthal angles, i.e. $\mathrm{EI}\left(\theta, \phi_2\right)/\mathrm{EI}\left(\theta, \phi_1\right)$, to estimate fracture weaknesses. Based on the expression of EI shown in equation 9, we emphasize that in the case of employing $\mathrm{EI}\left(\theta, \phi_2\right)/\mathrm{EI}\left(\theta, \phi_1\right)$ as input datasets only the normal and tangential fracture weaknesses are left as unknown parameters in the inversion problem.

To produce azimuthal EI datasets, we employ a Bayesian inversion algorithm to implement the inversion of input PP-wave seismic gathers without NMO correction based on the re-expressed convolution model shown in equation 10.

Assuming the independent and Gaussian noise and univariate Cauchy prior, we present the objective function J that can generate the EI vector $\mathbf{e}$ as

$$
J\left(\mathbf{e}\right) = \frac{1}{2\sigma_{\mathrm{n}}^2}\left(\mathbf{s} - \mathbf{A}\,\mathbf{e}\right)^T\left(\mathbf{s} - \mathbf{A}\,\mathbf{e}\right) + \sum_{i=1}^{2nl} \ln\left[1 + \frac{\left(\mathbf{e} - e_{\mathrm{c}}\right)^T\left(\mathbf{e} - e_{\mathrm{c}}\right)}{\sigma_{\mathbf{e}}^2}\right], \qquad (13)
$$

where σ_{n}^2 is the variance of noise, $\sigma_{\mathbf{e}}^2$ is a scale parameter related to the variance of $\mathbf{e}$, and e_{c} is the center of EI vector.

Differentiating the objective function with respect to $\mathbf{e}$ (i.e. $\frac{\partial J}{\partial \mathbf{e}}$) and setting the result of

$\frac{\partial J}{\partial \mathbf{e}}$ to zero, we obtain

$$\left(\mathbf{A}^T \mathbf{A} + \frac{2\sigma_{\mathrm{n}}^2}{\sigma_{\mathbf{e}}^2} \mathbf{Q}\right) \mathbf{e} = \mathbf{A}^T \mathbf{s}, \tag{14}$$

where

$$\mathbf{Q} = \begin{bmatrix} \frac{1}{1 + \frac{(\mathbf{e}_1 - e_{\mathrm{c}})^T (\mathbf{e}_1 - e_{\mathrm{c}})}{\sigma_{\mathbf{e}}^2}} & & \\ & \ddots & \\ & & \frac{1}{1 + \frac{(\mathbf{e}_n - e_{\mathrm{c}})^T (\mathbf{e}_n - e_{\mathrm{c}})}{\sigma_{\mathbf{e}}^2}} \end{bmatrix}_{2ln \times 2ln} . \tag{15}$$

With the estimated EI in hand, we next implement the inversion for unknown parameter vector $\mathbf{m}$ involving δ_{N} and δ_{T} using the first- and second-order derivatives of EI with respect to $\mathbf{m}$. In the case of two azimuthal angles (ϕ_1 and ϕ_k), l incidence angle and n reflection interface, we succinctly express the logarithm of difference between EI of ϕ_1, ϕ_2, ϕ_3 and ϕ_4 as

$$\mathbf{d} = \mathbf{G}\mathbf{m}, \tag{16}$$

where

$$\mathbf{d} = \begin{bmatrix} \log(\mathrm{EI}\,(t_1, \theta_1, \phi_k)/\mathrm{EI}\,(t_1, \theta_1, \phi_1)) \\ \vdots \\ \log(\mathrm{EI}\,(t_{n+1}, \theta_1, \phi_k)/\mathrm{EI}\,(t_{n+1}, \theta_1, \phi_1)) \\ \vdots \\ \log(\mathrm{EI}\,(t_1, \theta_l, \phi_k)/\mathrm{EI}\,(t_1, \theta_l, \phi_1)) \\ \vdots \\ \log(\mathrm{EI}\,(t_{n+1}, \theta_l, \phi_k)/\mathrm{EI}\,(t_{n+1}, \theta_l, \phi_1)) \end{bmatrix}_{l(n+1) \times 1},$$

$$\mathbf{G} = \begin{bmatrix} \mathbf{p}_{\mathrm{N}}\,(\theta_1, \phi_1, \phi_k) & \mathbf{p}_{\mathrm{T}}\,(\theta_1, \phi_1, \phi_k) \\ \vdots & \vdots \\ \mathbf{p}_{\mathrm{N}}\,(\theta_l, \phi_1, \phi_k) & \mathbf{p}_{\mathrm{T}}\,(\theta_l, \phi_1, \phi_k) \end{bmatrix}_{l(n+1) \times 2(n+1)},$$

$$\mathbf{m} = \begin{bmatrix} \boldsymbol{\delta}_{\mathrm{N}} \\ \boldsymbol{\delta}_{\mathrm{T}} \end{bmatrix}_{2(n+1) \times 1}, \tag{17}$$

in which

$$\boldsymbol{\delta}_{\mathrm{N}} = \begin{bmatrix} \delta_{\mathrm{N}}\,(t_1) \\ \vdots \\ \delta_{\mathrm{N}}\,(t_{n+1}) \end{bmatrix}_{(n+1) \times 1},$$

$$\boldsymbol{\delta}_{\mathrm{T}} = \begin{bmatrix} \delta_{\mathrm{T}}\left(t_1\right) \\ \vdots \\ \delta_{\mathrm{T}}\left(t_{n+1}\right) \end{bmatrix}_{(n+1)\times 1},$$

$$\mathbf{p}_{\mathrm{N}}\left(\theta_l, \phi_1, \phi_k\right)$$
$$= 2 \begin{bmatrix} \left(a_{\mathrm{N}}\left(t_1, \theta_l, \phi_k\right) - a_{\mathrm{N}}\left(t_1, \theta_l, \phi_1\right)\right) & & \\ & \ddots & \\ & & \left(a_{\mathrm{N}}\left(t_{n+1}, \theta_l, \phi_k\right) - a_{\mathrm{N}}\left(t_{n+1}, \theta_l, \phi_1\right)\right) \end{bmatrix}_{(n+1)\times(n+1)},$$

$$\mathbf{p}_{\mathrm{T}}\left(\theta_l, \phi_1, \phi_k\right)$$
$$= 2 \begin{bmatrix} \left(a_{\mathrm{T}}\left(t_1, \theta_l, \phi_k\right) - a_{\mathrm{T}}\left(t_1, \theta_l, \phi_1\right)\right) & & \\ & \ddots & \\ & & \left(a_{\mathrm{T}}\left(t_{n+1}, \theta_l, \phi_k\right) - a_{\mathrm{T}}\left(t_{n+1}, \theta_l, \phi_1\right)\right) \end{bmatrix}_{(n+1)\times(n+1)}.$$
$$(18)$$

To obtain the results of fracture weaknesses, we once again use the Bayesian inversion algorithm under the assumption of the Gaussian error between the modeled and input EI-related datasets and the univariate Cauchy prior, and the objective function is given by

$$J\left(\mathbf{m}\right) = \frac{1}{2\sigma_{\mathrm{error}}^2}\left(\mathbf{d} - \mathbf{G}\,\mathbf{m}\right)^T\left(\mathbf{d} - \mathbf{G}\,\mathbf{m}\right) + \sum_{i=1}^{2N} \ln\left[1 + \frac{\left(\mathbf{m} - m_{\mathrm{c}}\right)^T\left(\mathbf{m} - m_{\mathrm{c}}\right)}{\sigma_{\mathbf{m}}^2}\right], \quad (19)$$

where m_{c} is the center of unknown parameter vector.

EXAMPLE RESULTS

Accuracy and robustness

We first use a well log model to clarify how to generate seismic gathers without NMO correction and verify the stability and robustness of the proposed inversion approach. Figure 2 shows curves of P- and S-wave velocities α and β, density ρ, porosity ϕ and clay volume V_{clay}.

Using approximate relationships between anisotropic parameters and fracture weaknesses proposed by Bakulin et al. (2000) and empirical relationships between P- and S-wave velocities and anisotropic parameters given by Li (2006), we express fracture weaknesses as a function of wave velocities as

$$\delta_{\mathrm{N}} \approx \frac{0.6\,V_{\mathrm{clay}}\,\left(\alpha - 1.5\right)}{4.55 - 2.65\,V_{\mathrm{clay}}}\frac{1}{2g\left(1 - g\right)},$$
$$\delta_{\mathrm{T}} \approx \frac{1.34\,V_{\mathrm{clay}}\,\beta}{4.09 - 2.29\,V_{\mathrm{clay}}}.$$
$$(20)$$

In Figure 3, we show the normal and tangential fracture weaknesses calculated using P- and S-wave velocities and clay volume.
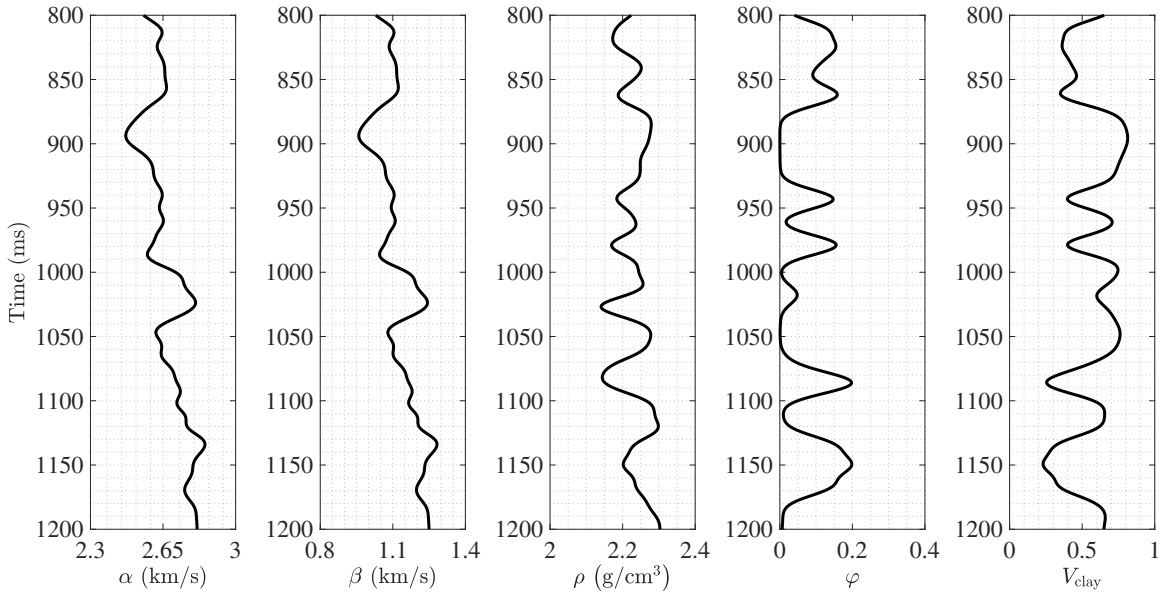
FIG. 2. Curves of P- and S-wave velocities α and β, density ρ, porosity ϕ and clay volume V_{clay} of well log model.
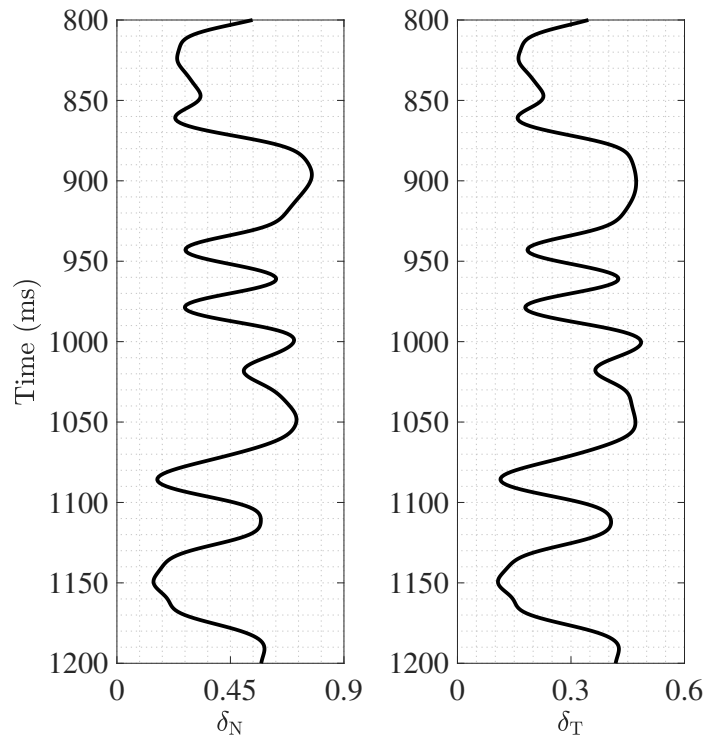
FIG. 3. The normal and tangential fracture weaknesses calculated using P- and S-wave velocities α and β and clay volume V_{clay}.

Using the re-expressed P-wave velocity, we first compute the NMO operator $\mathbf{N}$ of incidence angle θ of $5°$, $15°$ and $25°$ and azimuthal angle ϕ of $0°$ and $90°$, as shown in Figure 4. In Figure 4 d)-f) we observe that there is an approximately monotonic relationship between $\mathbf{N}(\theta, \phi = 90°)$ and P-wave travel time calculated at the normal incidence. In the case of ϕ of $0°$ the approximate monotonic relationship exists at small and middle incidence angles

(i.e. $\theta_1 = 5°$, and $\theta_2 = 15°$), as shown in Figure 4 a) and b); however, in the case of large incidence angles the NMO operator becomes more complicated, as shown in Figure 4 c).

Based on the re-expressed convolution model, we generate synthetic seismic gathers using a Ricker wavelet of dominant frequency 25 Hz, and we add Gaussian random noise to the generated synthetic seismic gathers to obtain the noisy seismic gathers of signal-to-noise ratio (SNR) of 2. In Figure 5, we show the obtained noisy synthetic seismic gathers of incidence angle of $5°$, $15°$ and $25°$ and azimuthal angle of $0°$ and $90°$. Compared with the computed NMO operators shown in Figure 4, we observe the NMO operators determine where seismic amplitudes are placed.

Using the proposed Bayesian inversion approach, we first implement the estimation of EI of different incidence and azimuthal angles using the obtained synthetic seismic data of SNR of 2. Figure 6 shows comparisons between true values and inversion results of logarithmic EI (LEI).

In Figure 6, we observe the inversion result of LEI can match the true value even in the case of SNR of 2, which illustrates the proposed approach may produce reliable inversion results of EI that can be used in the estimation of unknown parameters involving the normal and tangential fracture weaknesses.

With the estimated results of LEI in hand, we proceed to the inversion for fracture weaknesses using the proposed Bayesian algorithm. The input datasets are differences in the estimated LEI of two azimuthal angles ($\phi_1 = 0°$ and $\phi_2 = 90°$), as shown in Figure 7.

Comparisons between inversion results and true values of fracture weaknesses are shown in Figure 8. We observe there is a good match between inversion results and true values of δ_N and δ_T. It illustrates that reliable fracture weaknesses are obtained using the proposed two-step Bayesian inversion approach.

Real data

We proceed to the inversion for fracture weaknesses using real datasets that were acquired over a gas-bearing fractured reservoir. We first plot seismic data of zero offset in Figure 9. Well logging curve of P-wave velocity has been placed at CDP170. We observe in the location of fractured reservoir marked by the ellipse P-wave velocity exhibits relatively low values, and seismic reflection amplitudes are relatively strong.

We next plot seismic gathers of different angles of incidence ($\theta_1 = 4°$, $\theta_2 = 12°$ and $\theta_3 = 20°$) and azimuth ($\phi_1 = 0°$ and $\phi_2 = 90°$) that are obtained without NMO correction, as shown in Figure 10.

Comparing seismic gathers without NMO correction that are shown in Figure 10 a)-f), we observe both reflection amplitude and travel time vary with the angle of incidence and azimuth, which demonstrates features of AVAZ and VVAZ appear.

Following the proposed inversion workflow, we first implement the Bayesian inversion for LEI of different incidence and azimuthal angles using the corresponding seismic gathers
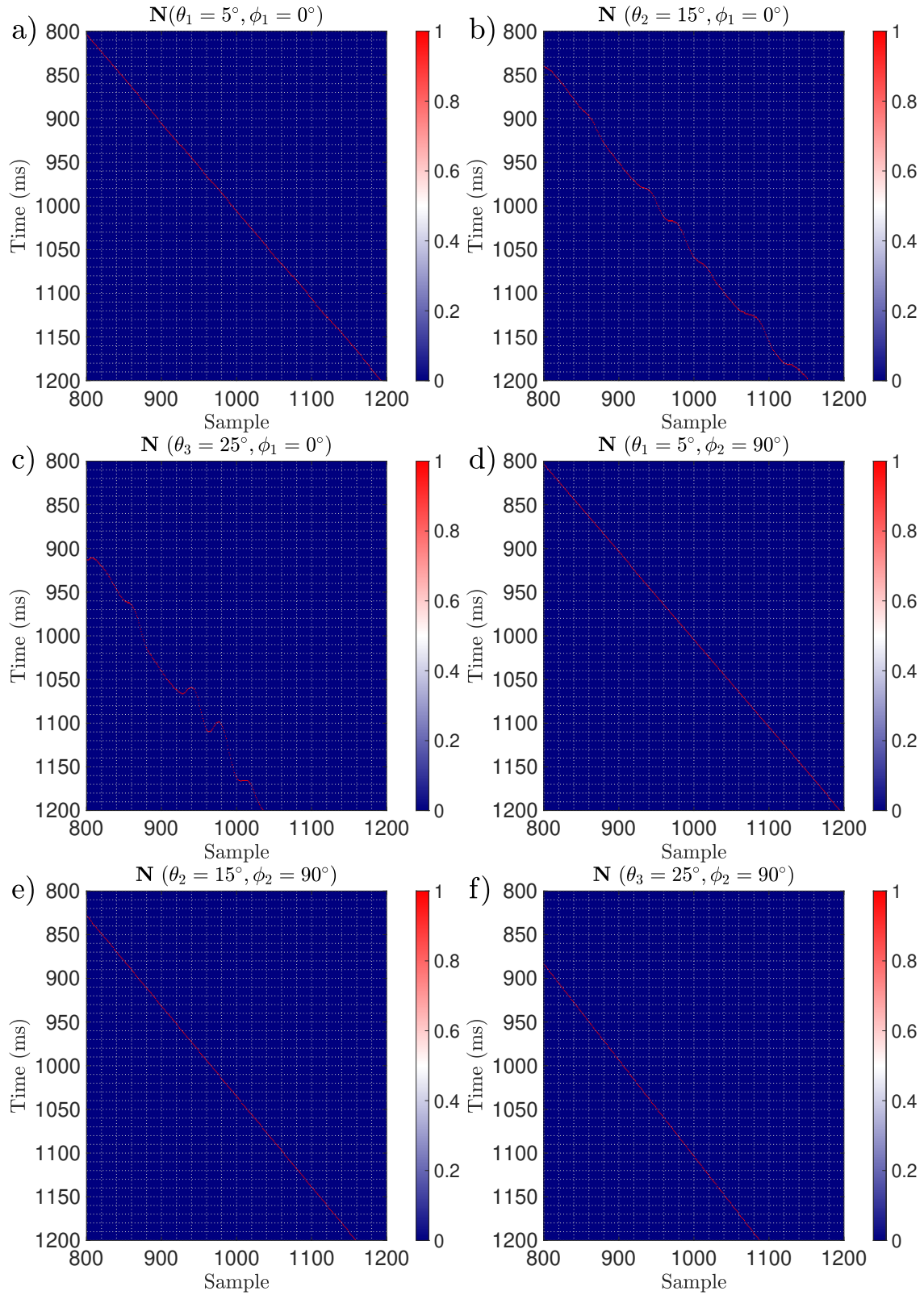
FIG. 4. NMO operators calculated in the case of different incidence and azimuthal angles. a) $\theta_1 = 5°$, $\phi_1 = 0°$; b) $\theta_2 = 15°$, $\phi_1 = 0°$; c) $\theta_3 = 25°$, $\phi_1 = 0°$; d) $\theta_1 = 5°$, $\phi_2 = 90°$; e) $\theta_2 = 15°$, $\phi_2 = 90°$; and f) $\theta_3 = 25°$, $\phi_2 = 90°$.
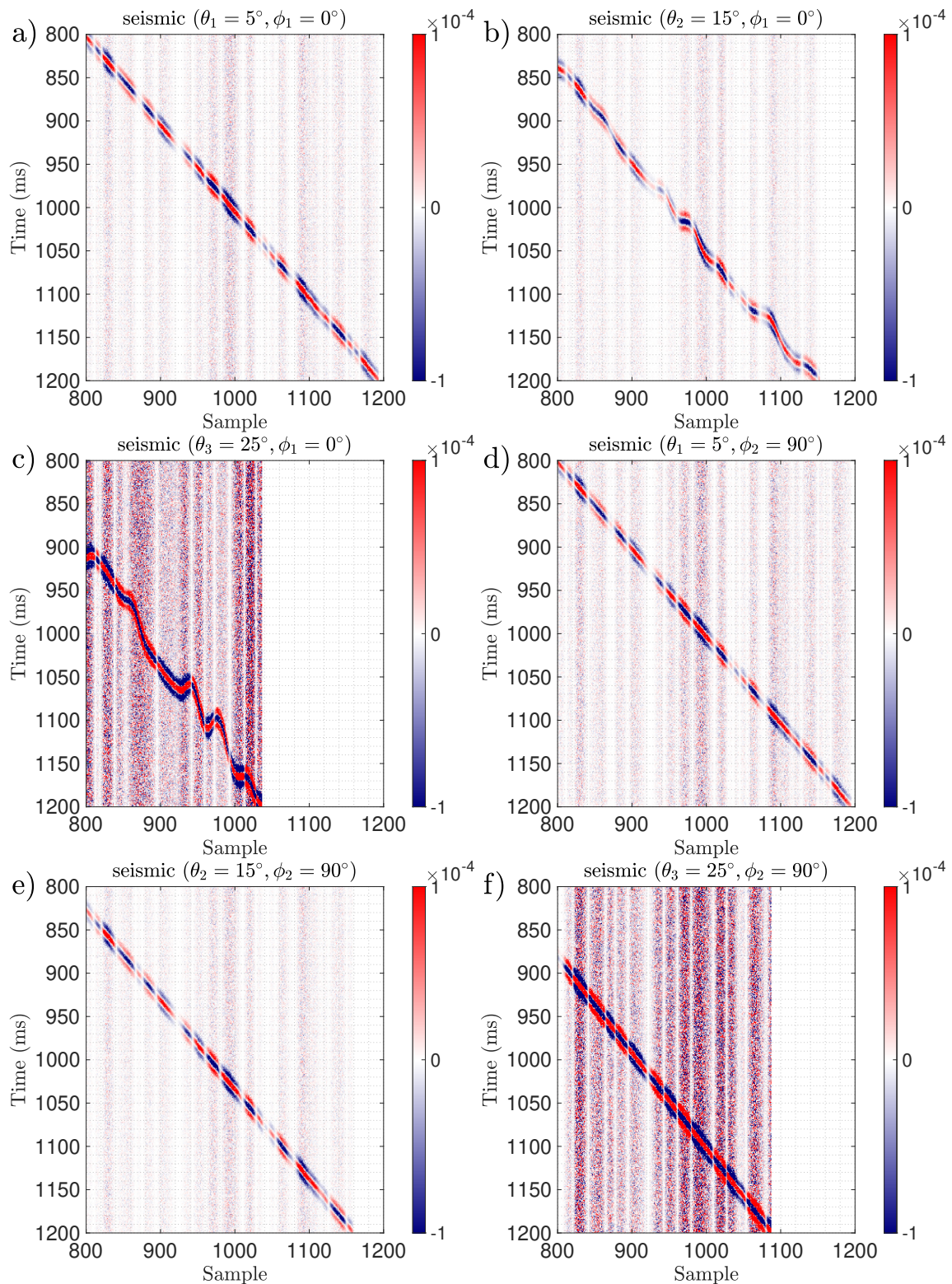
FIG. 5. Noisy synthetic seismic gathers of different incidence and azimuthal angles. a) $\theta_1 = 5°$, $\phi_1 = 0°$; b) $\theta_2 = 15°$, $\phi_1 = 0°$; c) $\theta_3 = 25°$, $\phi_1 = 0°$; d) $\theta_1 = 5°$, $\phi_2 = 90°$; e) $\theta_2 = 15°$, $\phi_2 = 90°$; and f) $\theta_3 = 25°$, $\phi_2 = 90°$.
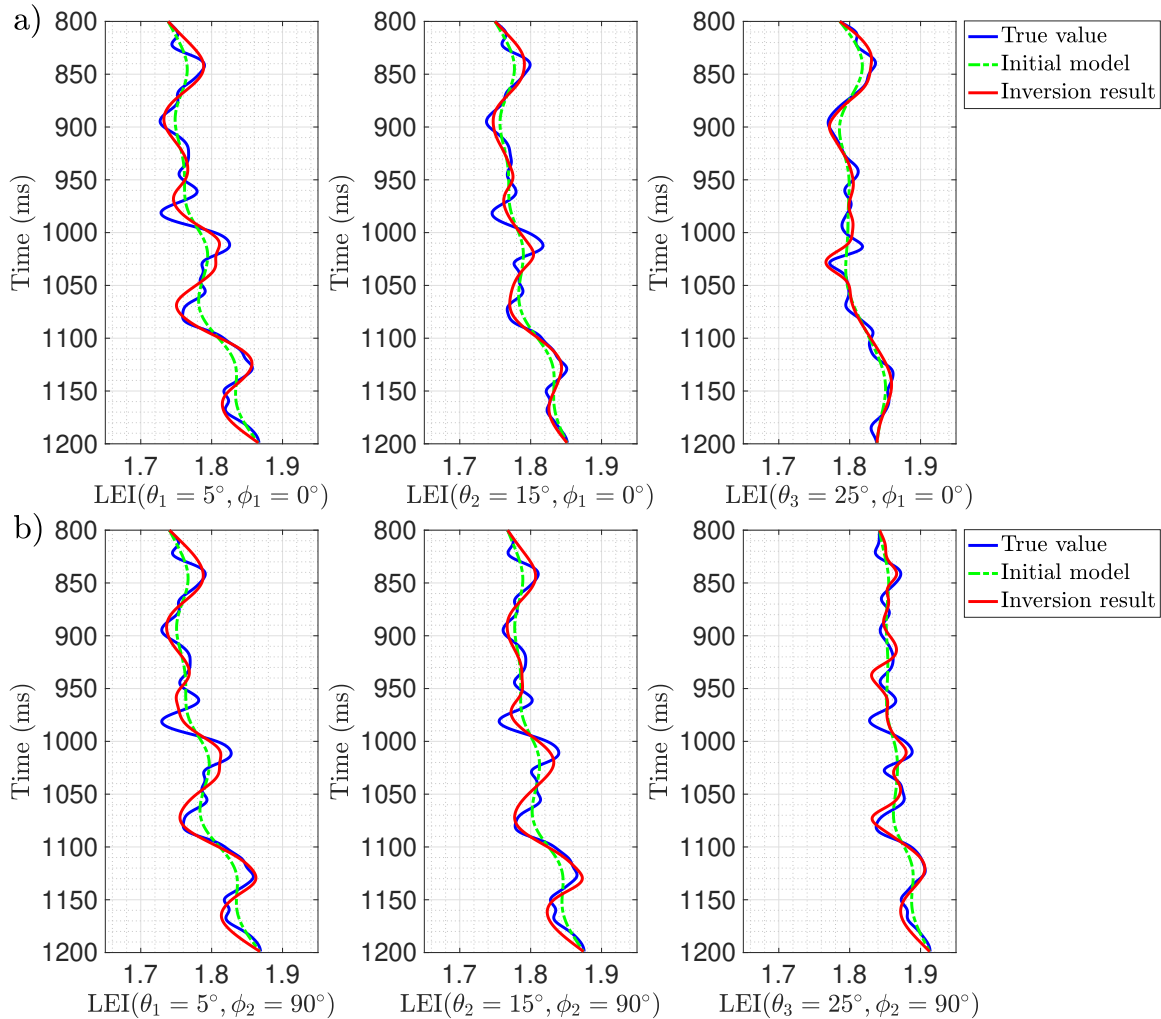
FIG. 6. Comparisons between true values and inversion results of logarithmic EI (LEI) of different incidence and azimuthal angles. Green curve represents the initial value of LEI, which is a smoothed version of the corresponding true value. a) $\phi_1 = 0°$; and b) $\phi_2 = 90°$.

without NMO correction. Inversion results of LEI of the angle of incidence ($\theta_1 = 4°$, $\theta_2 = 12°$ and $\theta_3 = 20°$) and azimuth ($\phi_1 = 0°$ and $\phi_2 = 90°$) are shown in Figure 11. We observe in the location of fractured reservoir the inverted LEI shows relatively low values.

Using the inversion results of LEI of different incidence and azimuthal angles, we may calculate the difference in LEI of ϕ_1 and ϕ_2, and with the calculated difference in LEI in hand, we may implement the estimation of fracture weaknesses δ_N and δ_T again using the Bayesian inversion approach. Inversion results of δ_N and δ_T are shown in Figure 12, and the curve of P-wave velocity obtained using well log data is also placed at CDP 170. We observe in the location of fractured reservoir both the normal and tangential fracture weaknesses show relatively high values, which is consistent with the feature that P-wave velocity exhibits relatively low values for fractured reservoirs.

By observing the inverted δ_N and δ_T, we can further infer that other locations where fracture weaknesses exhibit relatively high values may also be fractured reservoirs, as marked by the rectangle shown in Figure 12. To determine whether the inference is correct,
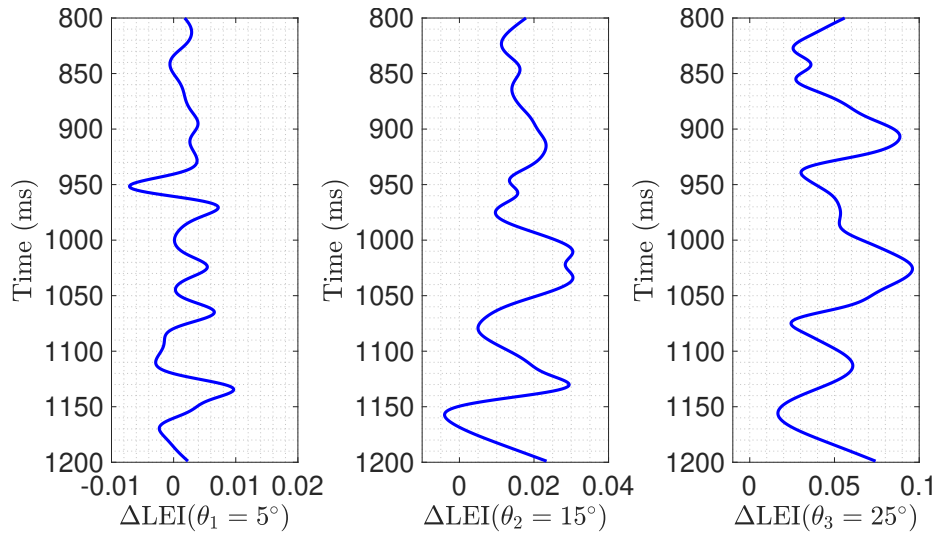
FIG. 7. Differences in the estimated LEI of azimuthal angles ϕ_1 and ϕ_2.
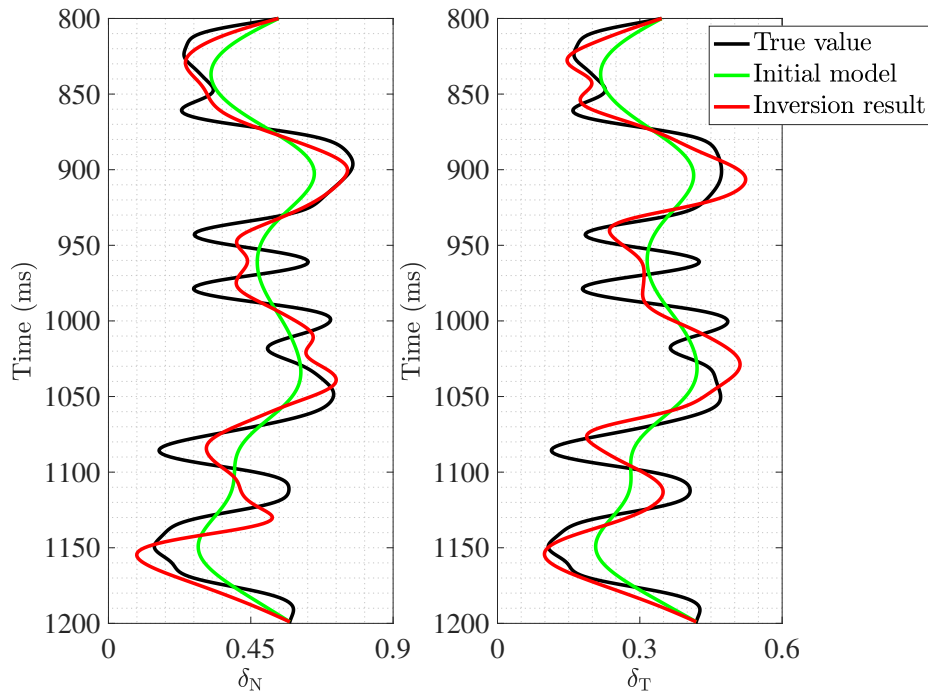
FIG. 8. Comparisons between inversion results and true values of fracture weaknesses.

more measurement data (e.g. well logging and drilling data) is required.

DISCUSSION

In seismic wave forward modeling and inversion, an incidence- and azimuthal-angle-dependent NMO operator N that is constructed using the P-wave velocity of isotropic background media (α) and fracture weaknesses (δ_N and δ_T) is indispensable. In the case of tests on synthetic seismic data, we directly utilize values of P-wave velocity and fracture weaknesses to generate the NMO operator of different incidence and azimuthal angles. However, in the real data case, P-wave velocity and fracture weaknesses of the entire Inline are miss-
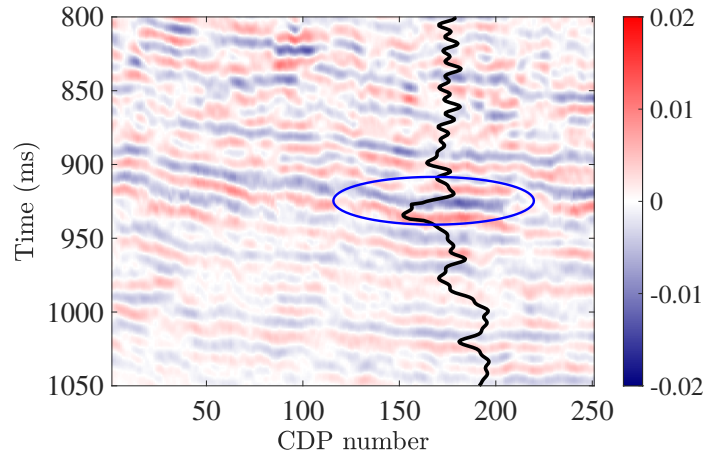
FIG. 9. Seismic gathers of zero offset. The curve represents P-wave velocity obtained using well log, and the ellipse indicates the location of fractured reservoir.

ing. In this section, we clarify how to construct the NMO operator in the case of applying the proposed inversion approach to seismic datasets to estimate logarithmic EI (i.e. LEI).

Using approximate relationships between anisotropic parameters and fracture weaknesses proposed by (Bakulin et al., 2000) and empirical relationships between P- and S-wave velocities and anisotropic parameters given by (Li, 2006), we roughly express fracture weaknesses as a function of wave velocities

$$
\begin{aligned}
\delta_{\mathrm{N}} &= \frac{0.6\, V_{\mathrm{clay}}\, (V_{\mathrm{P}} - 1.5)}{4.55 - 2.65\, V_{\mathrm{clay}}} \frac{1}{2g\,(1-g)}, \\
\delta_{\mathrm{T}} &= \frac{1.4\, V_{\mathrm{clay}}\, V_{\mathrm{S}}}{4.09 - 2.29\, V_{\mathrm{clay}}},
\end{aligned}
\tag{21}
$$

where V_{clay} is clay volume, and g is S-to-P modulus ratio.

Using P-wave velocity provided by well log and the estimated fracture weaknesses, we may construct the NMO operator at the position of drilling well.

Following Chen et al. (2017), we first estimate AVO anisotropic gradient using pre-stacked azimuthal seismic data, and then we roughly estimate fracture weaknesses based on relationship between the normal and tangential fracture weaknesses that obtained using well log data. Inversion of pre-stacked seismic data for P- and S-wave velocities and density is implemented. Using the roughly estimated fracture weaknesses and the inversion results of P-wave velocity, we may construct the NMO operator N for the entire Inline.

CONCLUSION

Based on the linear-slip model, we first re-express the incidence- and azimuthal-angle-dependent P-wave velocity as a function of fracture weaknesses that is related to fracture parameters (i.e. fracture density and infilling modulus). Using the solution of Zoeppritz equations, we derive an approximate P-to-P wave reflection coefficient and azimuthal elastic impedance (EI) in terms of the normal and tangential fracture weaknesses. Numerical example of a two-layered fractured model confirms the accuracy of the PP-wave reflection
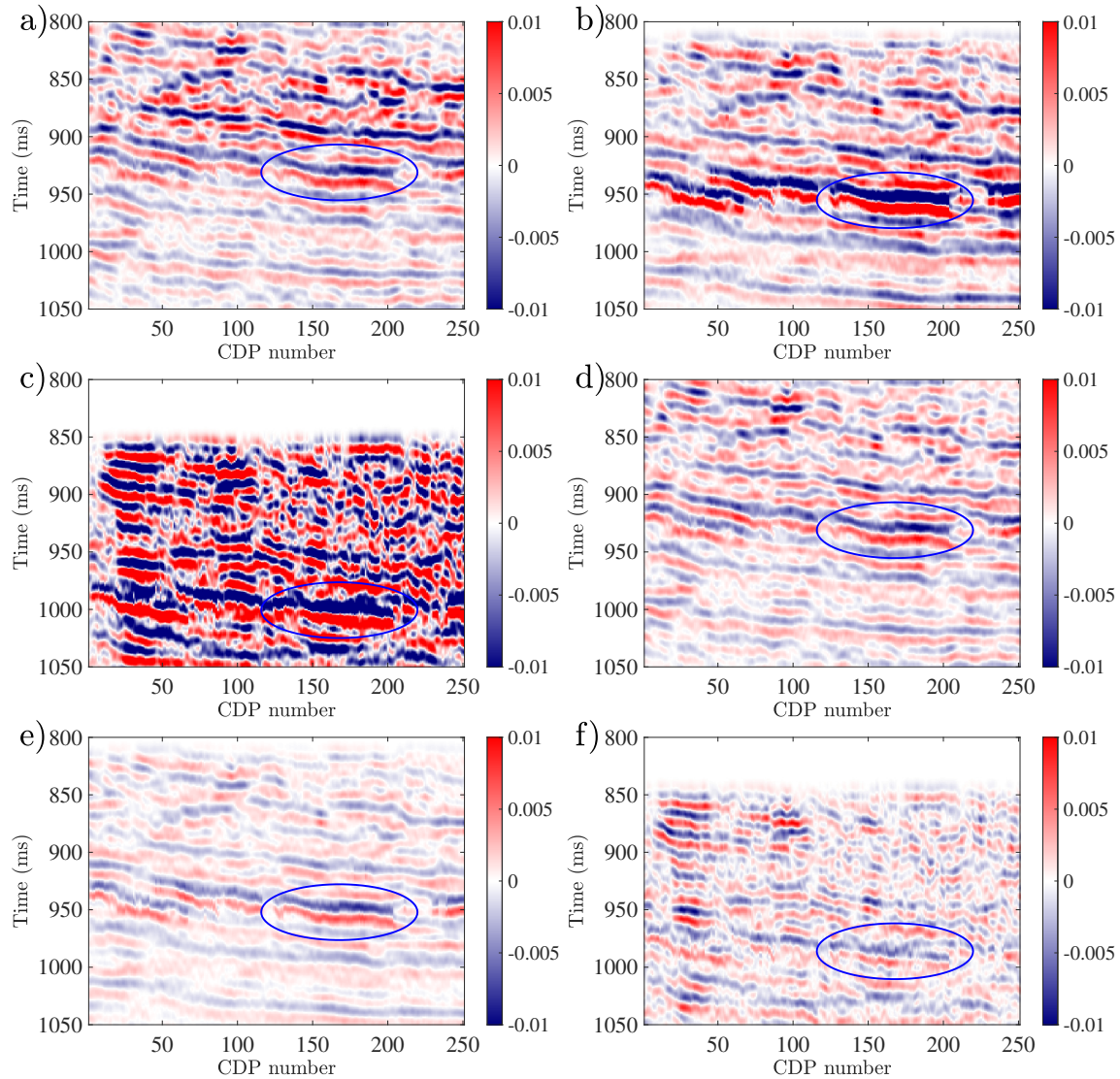
FIG. 10. Seismic gathers of different incidence and azimuthal angles. a) $\theta_1 = 4°$, $\phi_1 = 0°$; b) $\theta_2 = 12°$, $\phi_1 = 0°$; c) $\theta_3 = 20°$, $\phi_1 = 0°$; d) $\theta_1 = 4°$, $\phi_2 = 90°$; e) $\theta_2 = 12°$, $\phi_2 = 90°$; and f) $\theta_3 = 20°$, $\phi_2 = 90°$.

coefficient in the case of different incidence and azimuthal angles. Using the derived azimuthal EI, we introduce a NMO operator to re-express the convolution model to generate seismic gathers without NMO correction. Based on the convolution model, we establish a two-step inversion workflow involving: 1) the inversion for azimuthal EI using seismic gathers without NMO correction; and 2) the estimation of fracture weaknesses using azimuthal differences in the inverted EI datasets. In the case of test on synthetic seismic gathers of signal-to-noise ratio (SNR) of 2, we confirm the proposed inversion approach is robust and can produce stable inversion results of fracture weaknesses. Applying the proposed inversion approach and workflow to real datasets, we obtain reliable results of fracture weaknesses that may provide valuable information for the detection of potential fractured reservoirs.
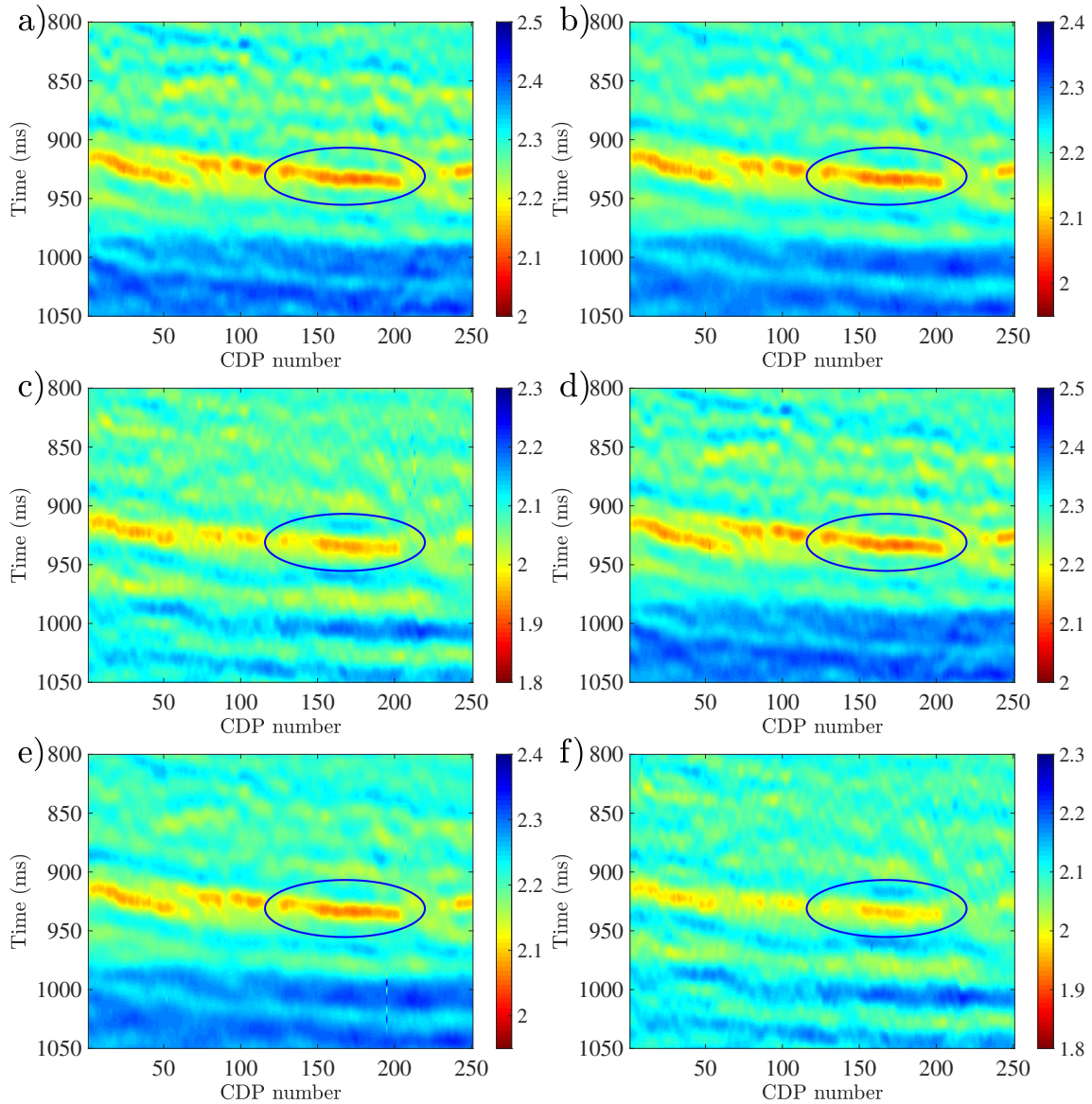
FIG. 11. Inversion results of logarithmic EI of incidence and azimuthal angles. a) $\theta_1 = 4°$, $\phi_1 = 0°$; b) $\theta_2 = 12°$, $\phi_1 = 0°$; c) $\theta_3 = 20°$, $\phi_1 = 0°$; d) $\theta_1 = 4°$, $\phi_2 = 90°$; e) $\theta_2 = 12°$, $\phi_2 = 90°$; and f) $\theta_3 = 20°$, $\phi_2 = 90°$. The location of fractured reservoir is marked by the ellipse.

ACKNOWLEDGMENTS

DATA AVAILABILITY

The data underlying this article will be shared on reasonable request to the corresponding author.
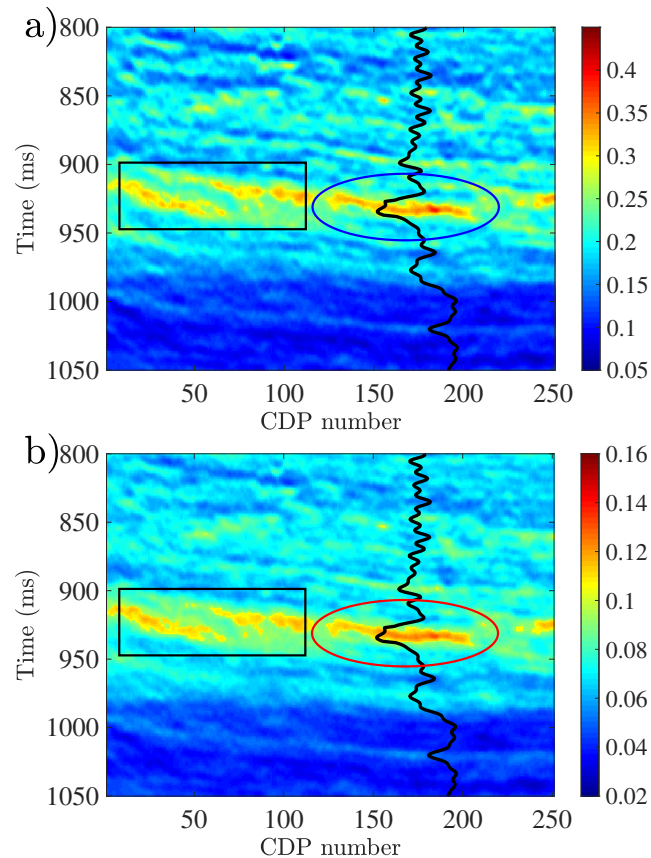
FIG. 12. Inversion results of fracture weaknesses. a) The normal fracture weakness δ_{N}; b) The tangential fracture weakness δ_{T}. The location of fractured reservoir is marked by the ellipse, and the curve represents P-wave velocity.

REFERENCES

Aki, K., and Richards, P. G., 2002, Quantitative seismology: University Science Books.

Bakulin, A., Grechka, V., and Tsvankin, I., 2000, Estimation of fracture parameters from reflection seismic data—Part I: HTI model due to a single fracture set: Geophysics, **65**, No. 6, 1788–1802.

Chen, H., Ji, Y., and Innanen, K. A., 2018, Estimation of modified fluid factor and dry fracture weaknesses using azimuthal elastic impedance: Geophysics, **83**, No. 1, WA73–WA88.

Chen, H., and Zhang, G., 2017, Estimation of dry fracture weakness, porosity, and fluid modulus using observable seismic reflection data in a gas-bearing reservoir: Geophysics, **38**, 651–678.

Chen, H., Zhang, G., Ji, Y., and Yin, X., 2017, Azimuthal seismic amplitude difference inversion for fracture weakness: Pure and Applied Geophysics, **174**, No. 1, 279–291.

Claerbout, J. F., 2004, Earth soundings analysis: Processing versus inversion: Blackwell Scientific Publications.

Downton, J., and Benjamin, R., 2010, Azimuthal simultaneous elastic inversion for fracture detection, *in* SEG Technical Program Expanded Abstracts, 263–267.

Hudson, J., 1980, Overall properties of a cracked solid: Mathematical Proceedings of the Cambridge Philosophical Society, **88**, No. 2, 371–384.

Ikelle, L. T., and Amundsen, L., 2018, Introduction to petroleum seismology: Society of Exploration Geophysicists.

Jenner, E., 2010, Modelling azimuthal nmo in laterally heterogeneous hti media: First Break, **28**, No. 9.

Li, Y., 2006, An empirical method for estimation of anisotropic parameters in clastic rocks: The Leading Edge, **25**, No. 6, 706–711.

Martins, J. L., 2006, Elastic impedance in weakly anisotropic media: Geophysics, **71**, No. 3, D73–D83.

Rüger, A., 1996, Reflection coefficients and azimuthal AVO analysis in anisotropic media: Ph.D. thesis, Colorado School of Mines.

Rüger, A., 1998, Variation of p-wave reflectivity with offset and azimuth in anisotropic media: Geophysics, **63**, No. 3, 935–947.

Schoenberg, M., and Protazio, J., 1992, "zoeppritz" rationalized and generalized to anisotropic media: Journal of Seismic Exploration, **1**, 124–144.

Schoenberg, M., and Sayers, C. M., 1995, Seismic anisotropy of fractured rock: Geophysics, **60**, No. 1, 204–211.

Tsvankin, I., 1997, Reflection moveout and parameter estimation for horizontal transverse isotropy: Geophysics, **62**, No. 2, 614–629.

Tsvankin, I., and Thomsen, L., 1995, Inversion of reflection traveltimes for transverse isotropy: Geophysics, **60**, No. 4, 1095–1107.

Zong, Z., Yin, X., and Wu, G., 2013, Elastic impedance parameterization and inversion with Young's modulus and Poisson's ratio: Geophysics, **78**, No. 6, N35–N42.

APPENDIX A. EXPRESSIONS OF FRACTURE WEAKNESSES δ_N AND δ_T

Expressions of fracture weaknesses δ_N and δ_T are proposed relating the penny-shaped crack model given by Hudson (1980) and the linear slip model given by Schoenberg and Sayers (1995). In the case of fluid-saturated fractures, the normal and tangential fracture weaknesses are expressed as

$$\delta_\mathrm{N} = \frac{4e}{3g\left(1-g\right)\left[1 + \frac{1}{\pi(1-g)}\frac{K_\mathrm{f}}{\mu\chi}\right]},$$
$$\delta_\mathrm{T} = \frac{16e}{3(3-2g)}, \tag{A.1}$$

where K_f is the effect bulk modulus of fluids in fractures, e is fracture density, and χ is fracture aspect ratio, respectively. In the case of fluids being a mixture of water and oil, the effective bulk modulus K_f is computed as

$$K_\mathrm{f} = 1/\left[S_\mathrm{W}/K_\mathrm{W} + \left(1 - S_\mathrm{W}\right)/K_O\right], \tag{A.2}$$

where S_W is water saturation, K_W and K_O are bulk moduli of water and oil, respectively.